PAPER Nr. : 18

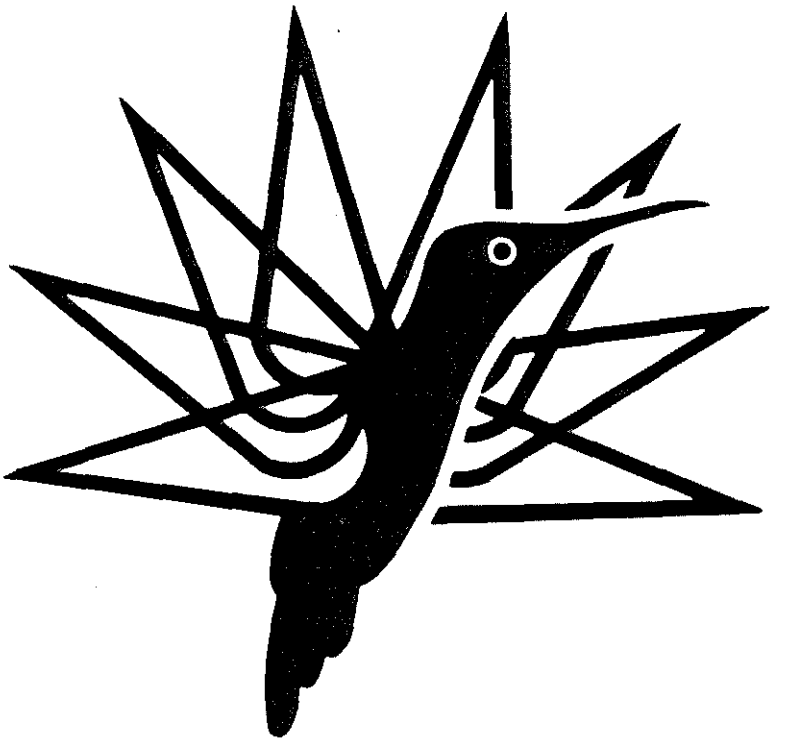

HELICOPTER MODEL ROTOR-BLADE VORTEX INTERACTION IMPULSIVE NOISE: SCALABILITY AND PARAMETRIC VARIATIONS

BY

W. R. SPLETTSTOESSER AND K. J. SCHULTZ
DFVLR, INSTITUT FÜR ENTWURFSAERODYNAMIK, ABTEILUNG TECHNISCHE AKUSTIK
BRAUNSCHWEIG, W. GERMANY

D. A. BOXWELL AND F. H. SCHMITZ
U.S. ARMY RESEARCH AND TECHNOLOGY LABORATORIES
AEROMECHANICS LABORATORY
NASA AMES RESEARCH CENTER, MOFFETT FIELD, CALIFORNIA, U.S.A.

TENTH EUROPEAN ROTORCRAFT FORUM

AUGUST 28 – 31, 1984 – THE HAGUE, THE NETHERLANDS

HELICOPTER MODEL ROTOR-BLADE VORTEX INTERACTION IMPULSIVE NOISE: SCALABILITY AND PARAMETRIC VARIATIONS

W. R. Splettstoesser and K. J. Schultz
DFVLR, Institut für Entwurfsaerodynamik, Abteilung Technische Akustik
Braunschweig, W. Germany

D. A. Boxwell and F. H. Schmitz
U.S. Army Research and Technology Laboratories
Aeromechanics Laboratory
NASA Ames Research Center, Moffett Field, California, U.S.A.

ABSTRACT

Acoustic data taken in the anechoic Deutsch-Niederlaendischer Windkanal (DNW) have documented the blade-vortex interaction (BVI) impulsive noise radiated from a 1/7-scale model main rotor of the AH-1 series helicopter. Averaged model-scale data were compared with averaged full-scale, in-flight acoustic data under similar nondimensional test conditions. At low advance ratios (μ = 0.164-0.194), the data scale remarkably well in level and waveform shape, and also duplicate the directivity pattern of BVI impulsive noise. At moderate advance ratios (μ = 0.224-0.270), the scaling deteriorates, suggesting that the model-scale rotor is not adequately simulating the full-scale BVI noise; presently, no proved explanation of this discrepancy exists. Carefully performed parametric variations over a complete matrix of testing conditions have shown that all of the four governing nondimensional parameters—tip Mach number at hover, advance ratio, local inflow ratio, and thrust coefficient—are highly sensitive to BVI noise radiation.

1. INTRODUCTION

Of all of the known sources of helicopter far-field noise radiation, rotor impulsive noise, when it occurs, tends to dominate the acoustic spectrum of most helicopters. The loud thumping or popping so characteristic of the two-bladed, single-rotor helicopter also occurs on helicopters with more rotor blades, but at a higher repetition rate that sounds more like a machine gun burst. Helicopter rotor impulsive noise is known to originate from two distinct aerodynamic events: high tip Mach numbers on the rotor's advancing side that cause near-transonic disturbances to radiate *high-speed impulsive noise*, and *blade-vortex interaction (BVI) impulsive noise* on the advancing and retreating sides of the rotor disk. A rather extensive review of this current research is given in reference 1.

Research of the past few years has successfully tied the details of the high-speed impulsive noise signature to the aerodynamic features of the transonic flow field surrounding the advancing blade of the high-speed helicopter (ref. 1). Recent model-scale and full-scale acoustic comparisons have shown that this source of noise can be successfully studied in model scale (refs. 1-3). Sensitivity studies have documented the dependence of high-speed impulsive noise on advancing-tip Mach number, and have shown that high-speed impulsive noise is relatively insensitive to the helicopter rotor wake or thrust effects.

The understanding of the specific origins and scalability of BVI noise are not as well understood. BVI noise is known to occur under conditions of landing and approach and during turns; it can even increase the noise level of single- or tandem-rotor helicopters in level flight (refs. 4-6). Past research and operational experience have tied the occurrence of BVI to interactions of the rotor blade with previously shed tip vortices. This alone makes BVI noise more difficult than high-speed impulsive noise to quantify, for the radiated noise is at least a function of blade-vortex geometry and vortex strength, as well as of blade airfoil characteristics.

From the viewpoints of research and the engineering development, it is very important to access whether the full-scale BVI phenomena can be duplicated to some measurable degree in model scale. Once this is demonstrated, model-rotor aerodynamic and acoustic changes can be explored with the confidence that those changes will yield results similar to those obtained on the full-scale rotor. A quantitative scaling comparison of this type was reported in reference 7 for the blade-vortex interaction problem of a two-bladed rotor. Full-scale acoustic data were gathered by using the in-flight far-field acoustic measurement technique pioneered by the Aeromechanics Laboratory (ref. 8). A quiet, fixed-wing aircraft (YO-3A), instrumented with microphones, was flown in formation with the subject helicopter to gather acoustic data over a matrix of test conditions known to produce BVI noise (refs. 5, 9). A 1/7-scale model of the main rotor was run under similar nondimensional conditions in one of the world's larger anechoic wind tunnels (CEPRA-19, France) and acoustic data were gathered for some of the same nondimensional flight conditions. For the low advance ratio reported, the comparison between model-scale and full-scale data was quite good, showing that in general it is possible to duplicate the full-scale BVI events in a model-scale test.

However, measurement and testing problems with both the full-scale and model-scale tests limited the data presented and prevented an in-depth comparison over a full range of testing conditions. The full-scale acoustic data could not be averaged by conventional procedures, because slowly varying station-keeping distances continuously time-shifted the acoustic data with respect to the one-per-rev trigger. The full-scale data that were presented were estimated to be "typical" in level and waveform for a chosen nondimensional condition. Unfortunately, tail-rotor periodic noise was also present for many of the test conditions and tended to confuse and distort some of the characteristic pulse shapes and amplitudes. The model-scale data were also affected by several measurement and testing uncertainties. The open test section of the CEPRA-19 wind tunnel was aerodynamically unsteady (2%-3% turbulence level), which caused the tip-path-plane of the rotor to wander slightly during a test condition. The acoustic properties of CEPRA-19 were influenced by the 3-m, hard-walled open-jet nozzle and thus were not totally in a nonreverberant field. However, the model-scale data were averaged to ascertain the general character of the radiated acoustic field in this nonideal environment. Because of these uncertainties, only the low-advance-ratio case ($\mu = 0.164$) was reported in reference 7.

In the present work, many of these measurement and testing problems have been avoided or solved, allowing comparisons of model- and full-scale data over a full range of testing conditions. A new method of averaging the in-flight BVI acoustic data has been developed that does not depend on fixed station-keeping distances and thus removes the tail-rotor periodic noise from the full-scale time-histories. The same 1/7-scale AH-1 model rotor was run in the free-world's largest open-jet anechoic wind tunnel (the German-Dutch wind tunnel, Deutsch-Niederlaendischer Windkanal (DNW)) to gather rotor-blade pressures and far-field radiated noise. The high-quality aerodynamic and acoustic environment of the DNW yielded high-quality, steady model-rotor acoustic data that are necessary to address adequately the quantitative comparisons between the model- and full-scale acoustic data over the full range of nondimensional testing conditions under which BVI noise is known to occur. In addition, the directivity of the radiating noise field is documented along with the more important trends of noise levels and temporal shapes with parametric variations. (The testing and subsequent data-reduction efforts are part of a continuing memorandum of understanding for cooperative research between the German and American governments.)

2. FULL-SCALE ACOUSTIC DATA

The full-scale data used in this comparison of model-scale and full-scale far-field acoustics were gathered using the in-flight technique developed by the Aeromechanics Laboratory (refs. 5, 9, 10). A quiet, fixed-wing aircraft (YO-3A), instrumented with an array of microphones, was flown in formation with the subject helicopter (AH-1) and stationary acoustic data were obtained over a full range of flight conditions (fig. 1). For BVI noise, selected conditions of forward velocity and rate of descent were flown with the microphone positioned directly ahead

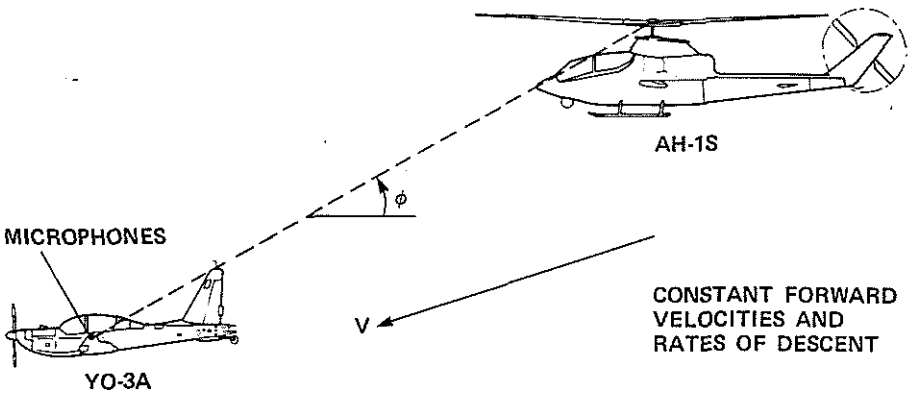

Fig. 1. Full-scale blade-vortex interaction acoustic measurement technique.

of the helicopter but approximately 30° below the rotor's tip-path plane. The major advantages of this technique are the long data records, the absence of ground reflections, and the ability to fly conditions that are conducive to producing BVI phenomena. Although the procedure has been used to evaluate the noise radiation of many helicopters, the full-scale data presented in this paper were taken on an AH-1S helicopter in 1978 and 1979 during two separate test programs and reported, in unaveraged form, in references 5 and 9. The data are repeatable and clearly define the BVI phenomena of interest.

3. MODEL-SCALE EXPERIMENTAL DESIGN

The model-rotor tests were performed in the DNW, an atmospheric wind tunnel of the closed-return type. It has three interchangeable, closed, test-section configurations and one open-jet configuration with a 6- by 8-m (19.7- by 26.2-ft) nozzle. In its open-jet configuration, the tunnel was designed for acoustic measurements with low background noise in an acoustically treated testing-hall volume of more than 30,000 m^3 (1.06×10^6 ft^3). The resulting good anechoic properties (cutoff frequency is 80 Hz) makes the DNW the free world's largest aeroacoustic wind tunnel. The tunnel also has excellent fluid dynamic qualities, with low unsteady disturbances over the total testing velocity range. The DNW characteristics most important for rotor aeroacoustic testing are given in appendix A of reference 2; additional information is provided in reference 11. The open-jet configuration with the 6- by 8-m contraction was used for the rotor tests reported here. The maximum wind velocity in this configuration is 85 m/sec (165 knots), which covers the full speed range of modern helicopters.

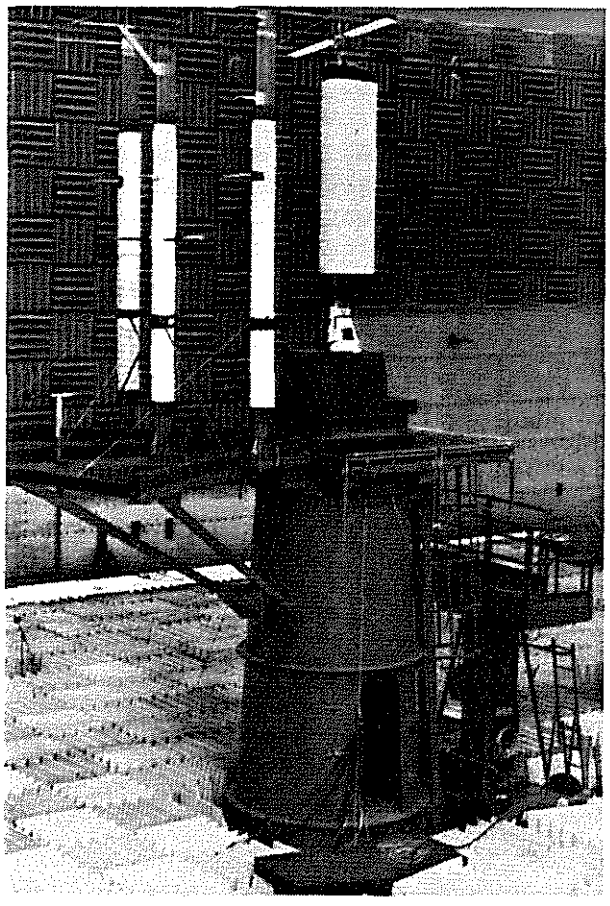

Figure 2. Rotor test stand mounted in the DNW open test section.

The model-rotor and microphone installation in the open test-section of the DNW are shown in figure 2. The Aeromechanics Laboratory's rotor test stand was mounted on a specially fabricated tower that placed the rotor on the tunnel centerline, 10 m (33 ft) above the testing-hall floor. The

in-flow microphones were supported by streamlined struts which were also attached to the tower structure. As shown in figure 2, the rotor test stand was shrouded with an aerodynamic fairing and wrapped with 25 mm of acoustic, open-celled foam to reduce sound reflections. An open-celled textile material (hospital bandage) was then wrapped around the foam to permanently secure it to the fairing. The same technique was used on the three main-microphone support struts located within the free jet. In the initial stages of testing, it was thought that it would be unnecessary to treat the microphone supports with foam; however, on-line acoustic calibrations of the test configuration showed reflections from the support struts that would have distorted the measured rotor acoustic signals (see appendix B of ref. 2). Additional acoustic calibrations with and without flow yielded the final test configuration shown in figure 2.

A total of 19 B&K 1/4-in. microphones (Type 4135) were distributed around the rotor, 10 of them in and 9 of them out of the open-jet core flow, as shown in figure 3. The locations of the in-flow microphones (Nos. 1-4, 6-10, and 15), typically 3.26 m (10.7 ft) from the rotor hub, were chosen to correspond to an average scaled microphone position of the full-scale acoustic tests reported in references 5 and 9. The out-of-flow microphones—most of which were located near the floor (Nos. 5, 22, and 16-19), above the rotor plane (Nos. 12 and 13), and toward the aft quadrant (No. 14) of the rotor—were used to gather additional information about directivity, distance, and shear-layer effects. Microphone calibrations were accomplished with B&K

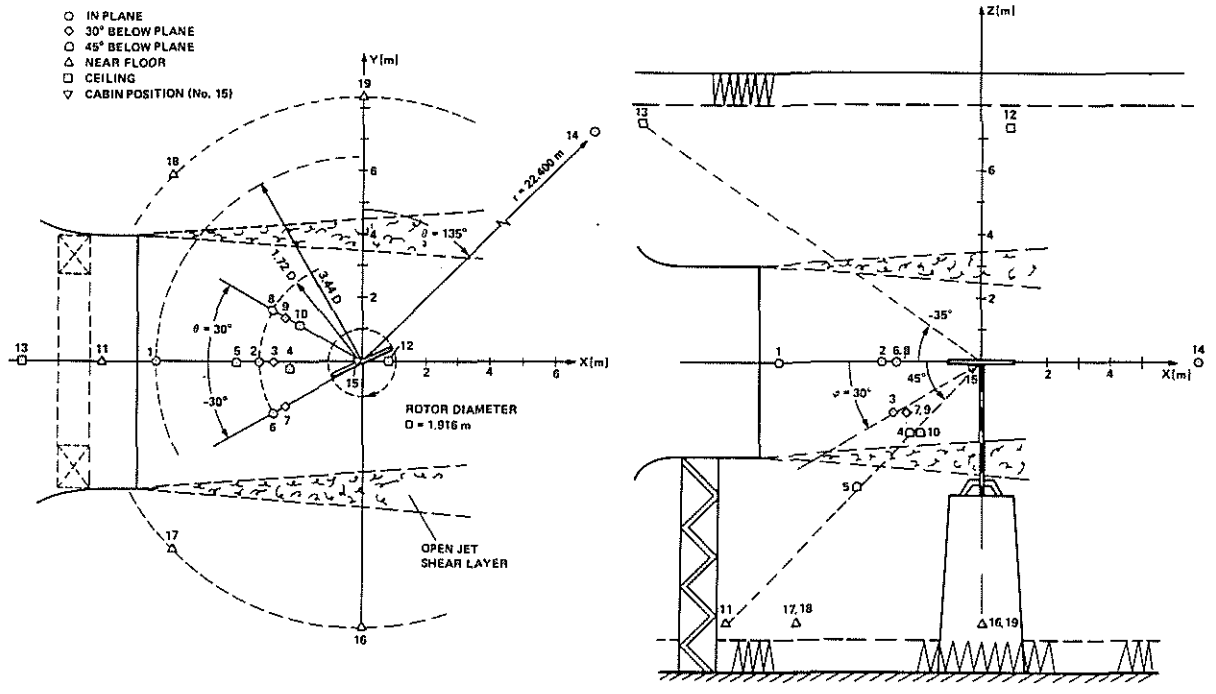

Figure 3. Microphone locations in the DNW.

pistonphones at the beginning or end of each recorded magnetic tape. For intermediate checks, the insert voltage method was applied.

The model-rotor blades were mounted on a teetering-hub assembly, with the collective, and the longitudinal and lateral cyclic rotor inputs provided by remotely controlled electric swashplate actuators. Tip-path-plane tilt was controlled directly through the cyclic, the shaft being rigidly mounted in the vertical position on the rotor stand. A six-component strain-gauge balance, comprising the top portion of the rotor stand, was used to monitor and record rotor thrust, drag, and pitching moments for each test condition. All the microphone signals and selected blade-pressure data were monitored on-line and, after proper signal conditioning, simultaneously recorded on three multichannel FM magnetic tape recorders; the recorders provided a total of 60 channels, which were set for a recording speed of 76.2 cm/sec (30 in./sec) and a frequency response of 20 kHz. IRIG-B time-code and rotor azimuth signals were recorded on each tape for synchronization purposes. During the 1-min data recording, two HP 5420A FFT analyzers were used to generate on-line instantaneous and averaged time-histories of selected microphones and pressure transducers. Wind-tunnel velocity, temperature, and dew point, as well as rotor speed, swashplate control inputs, and balance information, were processed on-line to yield nondimensional test conditions, using a portable HP 85 computer directly connected to the rotor balance. More detailed information about the setup and the pre-test calibrations performed are described in reference 2.

The model rotor blades used for the wind-tunnel testing did not exactly match the AH-1S 540 rotor system that was tested in full scale (refs. 5 and 9). Instead, the model rotor blades were designed to duplicate the AH1-OLS full-scale, pressure-instrumented blades, which also have recently been used for full-scale aerodynamics and noise testing by NASA. The thickness and chord of the full-scale 540 rotor blade were increased slightly (4% and 5%, respectively) to accommodate surface-pressure transducers, thus defining the OLS airfoil shape. The

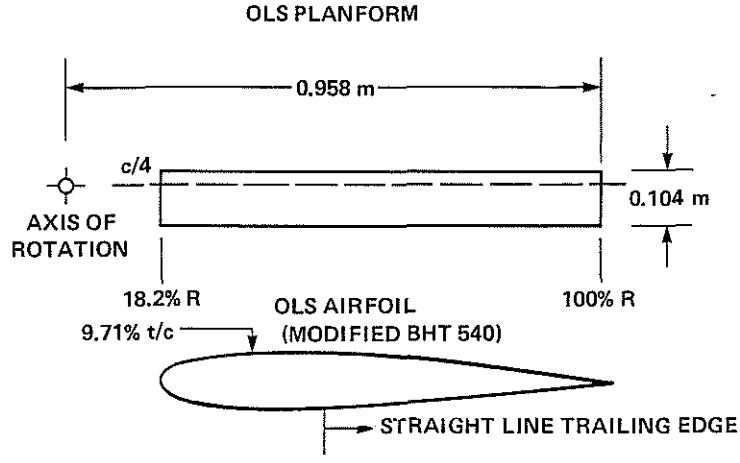

Figure 4. OLS blade characteristics.

1.914-m-diam (6.3-ft-diam) model rotor OLS blades are schematically shown in figure 4. Because the differences in thickness and chord between the full-scale 540 rotor and the model-scale OLS blades are small, no correction to either data set has been made in the following comparisons.

A photograph of the two-bladed, teetering, 1/7-scale (geometric) AH-1/OLS model rotor mounted on the six-component balance assembly in the anechoic DNW is shown in figure 5. Although not discussed in this paper, the model rotor was instrumented with 50 miniature pressure transducers to measure local surface-pressure distributions on the rotor blades while measuring the radiating noise. The location of some of the transducers can be seen near the leading edge and tip of the blade in the foreground. Also shown in figure 5 is a close-up view of the acoustic treatment of the rotor support stand.

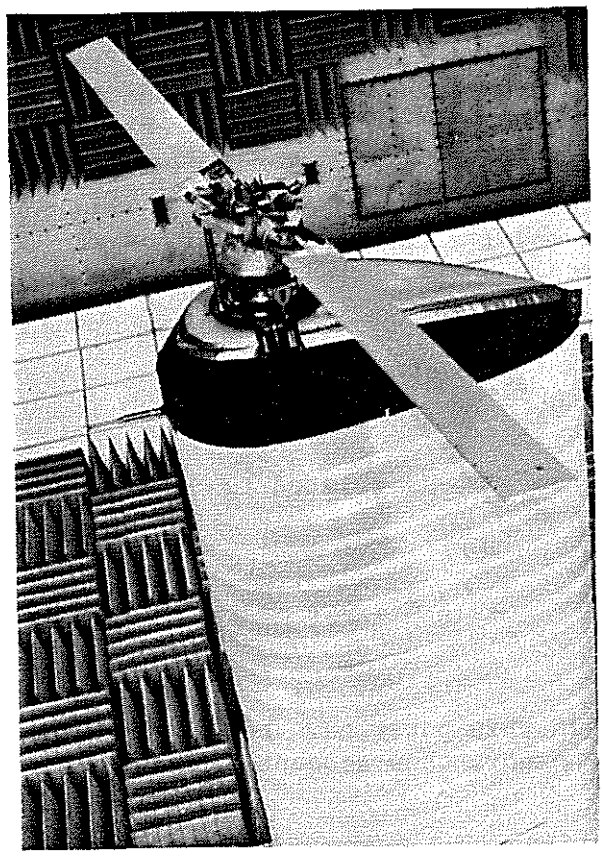

Figure 5. Two-bladed OLS model-rotor mounted on a teetering hub in the DNW.

4. ACOUSTIC SCALING PARAMETERS

When the fundamental equations of mass and momentum are written in an acoustic analogy form and nondimensionalized, four governing nondimensional testing parameters (M_H, the hover tip Mach number; μ, the advance ratio; C_T, the thrust coefficient; and α_{TPP}, the tip-path-plane angle) emerge along with geometric and time scaling. A complete

discussion of the nondimensionalization process is given in reference 1, and its application to the high-speed impulsive and BVI noise problems is given in references 2 and 7, respectively. Only the results of this procedure and its implications will be discussed in this paper.

The first and most obvious condition for comparing model-scale and full-scale acoustic data is geometric similarity. Thus, all model dimensions and geometric distances between the model rotor and microphone locations are $1/\gamma$ times the full-scale values:

$$\gamma = \frac{\text{full-scale length}}{\text{model-scale length}}$$

(For the data presented in this paper, $\gamma = 7$.) A second condition is that the model-scale and full-scale *hover tip Mach numbers* (M_H) be identical. This nondimensional parameter is the ratio of the rotor-tip speed at hover to the convection speed of the radiating acoustic waves, and it is known to be the dominant parameter of most rotor acoustic problems (ref. 1). Therefore, the geometrical reduction to model-scale factor γ must be offset by an increase of rotor-shaft rotational speed. However, speed-of-sound differences between model (a_{o_m}) and full-scale (a_o) conditions must be accounted for. Therefore, the rotational speed Ω_m of the model's rotor shaft (subscript m for model) is related to the full-scale shaft rotational speed by

$$\Omega_m = \gamma \frac{a_{o_m}}{a_o} \Omega$$

Also, a unit of model-scale time is related to full-scale time (eq. (C4) in ref. 2)

$$t_m = \frac{1}{\gamma} \frac{a_o}{a_{o_m}} t$$

All temporal data shown in this paper have been normalized by a rotor revolution or fraction thereof, thus accounting for time-scaling differences.

If all of the governing nondimensional parameters are matched, equation (C2) in reference 2 states that the acoustic pressure coefficient $C'_p(\bar{x},\bar{t})$ of the full-scale rotor is the same as $C'_{p_m}(\bar{x}_m,\bar{t}_m)$; that is,

$$C'_p(\bar{x},\bar{t}) = \frac{P'(\bar{x},\bar{t})}{\rho_o a_o^2} = \frac{P'_m(\bar{x}_m,\bar{t}_m)}{\rho_{o_m} a_{o_m}^2} = C'_{p_m}(\bar{x}_m,\bar{t}_m)$$

If, as is normally the case, dimensional pressure time-histories from two separate tests are to be compared, and in which all the governing nondimensional parameters have been matched, it is necessary to adjust the pressure levels to account for differences in $\rho_o a_o^2$, which is

proportional to the ambient pressure P_o. For convenience and in concert with past wind-tunnel acoustic practices, all acoustic data presented in this report will be referred to ISA standard day, sea-level pressure (indicated by an asterisk). Thus, model-scale pressures measured during wind-tunnel testing become in terms of ambient pressure ratio

$$P'^*_m(\bar{x}_m,\bar{t}_m) = \frac{P'_m(\bar{x}_m,\bar{t}_m)}{\rho_{o_m} a^2_{o_m}/\rho^*_o a^{*2}_o} = \frac{P'_m(\bar{x}_m,\bar{t}_m)}{P_{o_m}/P^*_o}$$

Because the DNW is located near sea level and because normal operating conditions were always close to the ISA standard day, only small pressure ratio corrections P_{o_m}/P^*_o were necessary for the model acoustic data presented in this paper. Similar correction procedures are necessary for flight-test data. Again, all acoustic data are referred to ISA standard day, sea-level pressure by

$$P'^*(\bar{x},\bar{t}) = \frac{P'(\bar{x},\bar{t})}{\rho_o a^2_o/\rho^*_o a^{*2}_o} = \frac{P'(\bar{x},\bar{t})}{P_o/P^*_o}$$

Since acoustic data were gathered at varying pressure altitudes, corrections were not insignificant for flight-test data (P_o/P^*_o of the order 0.7 to 0.8).

Besides scaling blade geometry and geometric distances between the rotor and the measurement microphones, hover tip Mach number (M_H), and time-scaling of the acoustic waveforms, there are at least three additional nondimensional parameters that should be duplicated if model-scale acoustic data are to match full-scale data. One of the most important is the *advance ratio* μ, defined to be the ratio of the helicopter's forward speed of translation divided by the tip speed of the main-rotor at hover. To first order, it controls the large-scale geometrical patterns of the BVI phenomena. If it is assumed that induced-wake distortions are small, the in-plane projection of the locus of points traced out by each tip of the rotating blades becomes a simple epicycloical tip-vortex pattern (refs. 1 and 6). When viewed from above, the rotor appears to slice through the epicycloid patterns of previously shed tip vortices. The resulting loci of interactions determine the number and strength of the blade-vortex encounters and, thus, strongly influences the radiated noise. Together, the advance ratio and the hover tip Mach number completely specify the rotor's advancing-tip Mach number M_{AT}, that is,

$$M_{AT} = (1 + \mu)M_H$$

and the Mach number of the moving acoustic sources in the radiation direction, M_r. In effect, all Mach numbers associated with the large-scale geometry of BVI are governed by the two nondimensional parameters, μ and M_H.

Judicious matching of the third and fourth nondimensional parameters—*thrust coefficient* C_T and nondimensional inflow λ— is necessary to duplicate the aerodynamic and acoustic pressure coefficients of the model-scale and full-scale experiments.

For a geometrically scaled rotor, the thrust coefficient governs the local angle of attack of the rotor blade and thus the steady-pressure field. In addition, it affects the average strength of the shed tip-vortex, thus directly influencing the unsteady-pressure field as well. The nondimensional inflow $\lambda = \mu\ (-\alpha_i + \alpha_{TPP})$ also affects the magnitude of the unsteady pressures by governing the vertical separation between the vortex and the rotor blade at the time of an encounter. In a rigorous sense, this parameter should scale over the portion of the rotor disk where BVIs occur. However, it is often assumed that by scaling geometric properties and C_T, an average value in space and time of the induced angle α_i at the rotor disk governs the interaction problem ($\alpha_i \sim C_T/\mu$). Therefore, if C_T and μ are duplicated in the model- to full-scale test, the nondimensional inflow is controlled by the rotor's *tip-path-plane angle*, α_{TPP}, and replaces the nondimensional inflow as the fourth nondimensional test variable.

In normal, unaccelerated level flight, the helicopter pilot must tilt the rotor tip-path-plane ($\alpha_{TPP} \equiv$ the angle between the plane of the rotor tips and the incoming velocity vector; positive for rearward tilt) to balance the drag of the vehicle at each velocity. The result is an increasingly negative tip-path-plane angle with increasing forward velocity. In a climb, the rotor must be tilted farther forward ($-\alpha_{TPP}$) both to balance drag and to oppose gravity, whereas in a descent the rotor must be tilted rearward ($+\alpha_{TPP}$). The strongest BVIs are known to occur in the descent condition, when the tip-path-plane angle is positive, forcing sections of the shed tip-vortices close to or into the rotor's tip-path-plane (refs. 5 and 6). Similar tip-path-plane angles must be flown in the wind tunnel to generate similar model-scale operating conditions.

Tip-path-plane angle (α_{TPP}) is not usually used as a piloting indicator when flying helicopters. Rate of climb (R/C), as well as forward velocity and engine torque, is the variable normally used by pilots to judge the state of the helicopter's performance. However, tip-path-plane angle can be related to rate of climb in steady-state flight through a simple balance of longitudinal forces. For small angles, it can be shown that

$$\alpha_{TPP} \simeq \frac{-D}{W} + \gamma_f \tag{1}$$

where

$$\frac{D}{W} = \left(\frac{f_e}{2AC_T}\right)\mu^2$$

$$\gamma_f = \tan^{-1}\frac{R/C}{60\ V}$$

V ≡ forward velocity of the helicopter

f_e ≡ equivalent wetted drag area of the helicopter

A ≡ rotor disk area of the helicopter

This approximate relation between tip-path-plane angle and rate of climb is plotted in figure 6 versus advance ratio for the AH-1S helicopter (f_e = 14 ft^2, A = 1520 ft^2, and C_T = 0.0054) for families of constant rates of climb and descent. Also shown on the same figure (indicated by the crosses) are calculated values from the C-81 trim computer program for the S-model Cobra helicopter (ref. 12). The simple balance-of-force model and the C-81 trim program agree quite well, lending confidence to the assumption that the simple relationship given by equation (1) is consistent over the matrix of flight conditions tested.

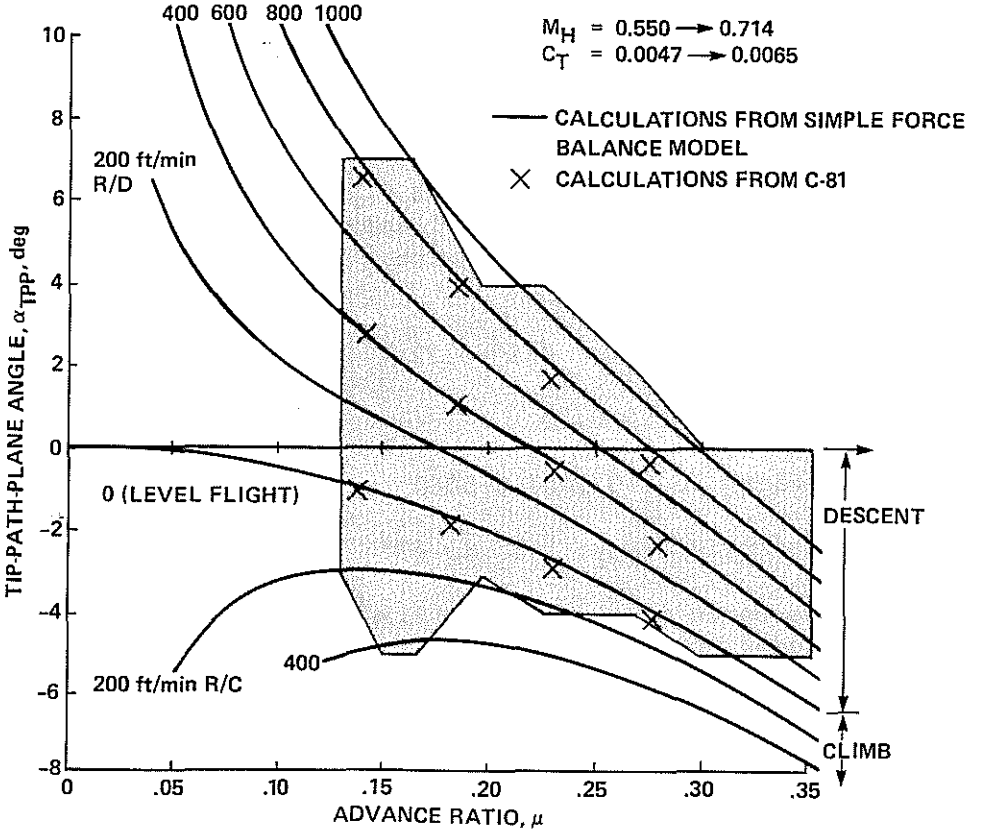

Figure 6. OLS model testing envelope.

However, the accuracy with which these conditions can be maintained during the testing is quite different for the model and full scale. In the low turbulence environment of the DNW, it is quite easy to establish steady-state testing conditions for the rotor. Tip-path-plane angles are equivalent to the longitudinal flapping angles with respect to the vertical shaft. Lateral tip-path-plane tilts were set to zero during all model-scale testing. All is not that easy in full-scale testing. Small but noticeable control movements were necessary during runs in order to help maintain a correct station-keeping position. These control inputs tended to make the full-scale data more unsteady, even though the pilots were given specific instructions not to hold station-keeping position too tightly once the target distance was acquired. There is also some question about how each pilot trimmed the helicopter. It is possible to arrive at steady level flight in a helicopter with or without sideslip, thus tending to make the full-scale conditions flown during the testing somewhat variable from run to run. The net result is that the equivalence shown in figure 6 should be viewed skeptically, keeping in mind that any full-scale conditions flown were mean values. To ensure that the full-scale BVI phenomena were duplicated in model-scale, a range of chosen tip-path-plane angles was flown in sweeps of 0.5° increments at chosen advance ratios.

The matrix of test conditions for which it was possible to gather both in-flight and model-scale acoustic data is shown in figure 6 by the shaded area. For these combinations of advance ratio and tip-path-plane angle, the thrust coefficient and hover tip Mach number were fixed at the nominal full-scale values: $C_T = 0.0054$ and $M_H = 0.664$, respectively. The data presented in this paper emphasize blade-vortex interaction impulsive noise and thus encompass many test points in the left of the shaded region (i.e., low to medium advance ratios). However, a significant amount of model testing time was spent exploring the effect of nondimensional parametric changes on BVI impulsive noise as well. The ranges of the four governing nondimensional parameters considered were as follows:

Hover tip Mach number M_H: 0.55-0.72

Advance ratios μ: 0.13-0.35

} (M_{AT} = 0.62-0.94)

Thrust coefficient C_T: 0.0047-0.0080

Tip-path-plane angle α_{TPP}: -5° to +7°

Most of the data were taken in descending flight at lower advance ratios where BVI noise is known to be of primary concern.

5. MODEL-SCALE AND FULL-SCALE COMPARISONS

In previous in-flight measurement investigations of full-scale rotor BVI impulsive noise (refs. 5, 7, and 9), it was impossible to use signal averaging to improve the signal-to-noise ratio of the periodic noise phenomena. During a typical data run, the nominal separation distance between the subject helicopter and the noise-measurement platform (YO-3A aircraft) continuously changes. Even though these changes

are quite small (estimated to be ±3 ft), they correspond to changes in time of about ±3 msec. In effect, the 1/rev trigger which could be used to average the data has a ±3-msec random delay. Because most of the BVI impulses are of the order of 1 msec wide, a processor that uses the rotor 1/rev signal to average the in-flight data is not effective.

These problems were overcome for high-speed impulsive noise by using the impulses themselves to construct a trigger signal (refs. 2, 3, and 8). In general, developing a good triggering signal is quite straightforward, if the event of interest is high in level and if it is periodic, two of the known qualities of high-speed impulsive noise. This same procedure was used to average the BVI noise presented in this paper. Signal conditioning methods were needed to pre-process the lower levels of the negative pressure spike associated with high-speed impulsive noise. A trigger signal was constructed and used to average the full-scale acoustic data to improve the signal-to-noise level and to define more completely the character of the full-scale BVI waveform.

The results of this new averaging procedure are illustrated in figure 7(a) for a typical set of conditions known to produce BVI impulsive noise. Two unaveraged signals are shown for one complete rotor revolution. The uppermost one represents the most intense BVI pulse and the middle one represents the weakest BVI pulse that was measured during a full-scale run. In all cases, BVI pulses occur slightly before the wide, negative, high-speed impulsive-noise pulse. The general unsteadiness of the full-scale BVI noise data is clearly demonstrated. Fifty percent fluctuations of peak impulsive-noise amplitude can occur during the run, suggesting that very steady flight at any full-scale condition did not really exist. In both the unaveraged full-scale data, tail-rotor periodic noise is also present, tending to confuse the interpretation of waveform details. Averaging the data (bottom graph in fig. 7(a)) using this new averaging procedure improves the interpretation tremendously. Not only has the periodic tail-rotor noise been reduced in level until it is not observable, but the lower-level character of the BVI acoustic full-scale pulse is visible for the first time. Because the data were averaged by triggering on the first high-speed negative impulse, the first half of the average yields better signal-to-noise levels than the second half. In the data that follow, only the first half impulse of the full-scale data is compared with the model scale. The questions of blade-to-blade pulse amplitude and shape variability remain for additional work.

Instantaneous and averaged model-scale data for approximately the same set of nondimensionalized conditions are shown in figure 7(b). Because no dramatic differences among the maximum, minimum, or average pulse time-histories was observed, only one instantaneous pulse is plotted. The extremely steady environment of the DNW shows that the average pulse level and waveform are quite representative of any single record.

The comparison of the model-scale and full-scale averaged data for this one flight condition (the lower graphs in figs. 7(a) and 7(b)) is quite remarkable. Even the smaller details of the acoustic waveforms agree fairly well in character and level. In particular, the smaller impulses that appear superimposed upon the negative spike of the

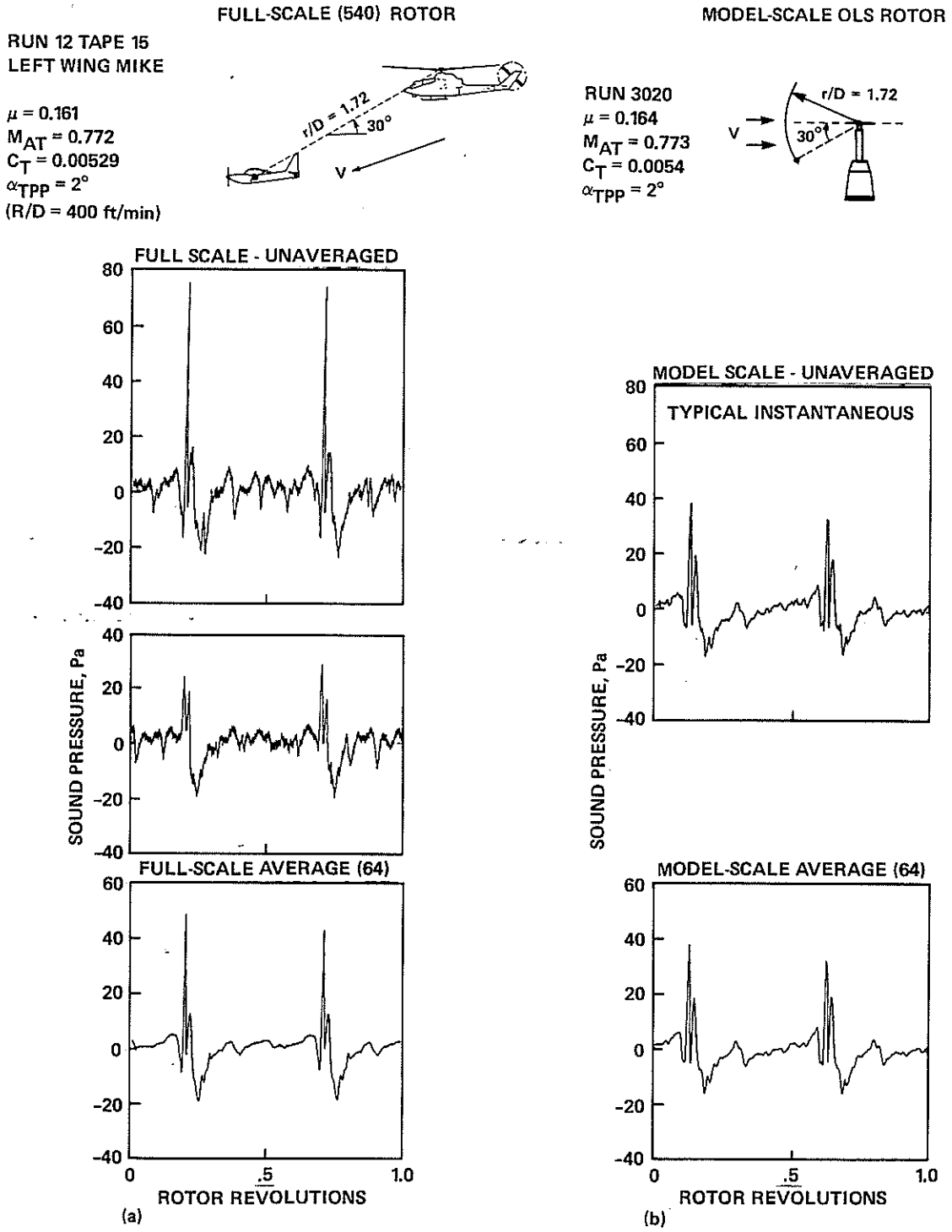

Figure 7.- Comparison of unaveraged and averaged sound pressure time-histories for one rotor revolution.

high-speed impulsive noise are duplicated. These were also seen in the model-scale data (ref. 7) taken in the CEPRA-19, but in that instance they were thought to be due to impulse reflections from the tunnel nozzle. Their appearance in both the model-scale DNW data and the full-scale data shown here suggests that another impulsive noise source is being measured—perhaps BVI on the retreating side of the rotor disk.

The comparison of model-scale and full-scale averaged acoustic data is shown in figures 8(a) and 8(b) for a range of longitudinal and lateral directivities for a low-speed descent condition known to produce BVI. The general comparisons of distinct acoustic events for one half a rotor revolution are quite good for all of the microphone locations shown. Some small discrepancies in averaged amplitudes of specific BVI events are observed at certain microphone locations. These are believed to result from aircraft control difficulties encountered in full-scale flight tests and from the generally limited accuracy of full-scale testing. Some of the measurement differences between full scale and model scale are noted on the figure at each scaled microphone location. In the plane of the rotor, where high-speed impulsive noise is most intense, the high-speed impulsive noise portion of the waveform (large negative pulse) is slightly larger in model scale than in full scale. This is due, in part, to the small increases in scaled thickness of the OLS model blade section when compared to the standard full-scale 540 section (ref. 2). Because the main interest here is in BVI noise, no correction for this effect has been made in the data shown. As reported by many researchers for this flight condition, BVI noise is seen to be most intense about 30° to 45° below the tip-path plane and directly ahead of the helicopter (refs. 5 and 8).

The general unsteadiness of the full-scale BVI acoustic data suggests that steady-state trimmed flight in formation with the YO-3A aircraft was difficult to achieve. The small control inputs needed to maintain station-keeping had the effect, to some degree, of changing the state of the helicopter during any particular data run. To account for these possible inaccuracies, the model-scale testing was performed over a range of nondimensional test variables. In particular, the model-scale tip-path-plane angle was varied in increments of 0.5° to ensure that a full-scale event would be captured in the model-scale test. These were compared with the full-scale data taken over a range of rates of climb. This comparison is shown in figures 9-12 for four advance ratios known to produce BVI (μ = 0.164, 0.194, 0.224, and 0.270).

In the top halves of figures 9-12, the model-scale and full-scale averaged acoustic data for one half of a rotor revolution are compared. The simple force-balance drag model equivalence between rotor tip-path-plane angles and rates of descent is indicated to the right of the full-scale rates of descent axis. In the lower half of each figure, the largest values of BVI are plotted on a magnified scale so that key differences between the model-scale and full-scale results can be emphasized. The model-scale results presented are for the 45°-down microphone position. As discussed in reference 2, it was felt that most of the full-scale 30° longitudinal positions flown were actually closer to 45° below the rotor's tip-path-plane. As shown in figure 8, at the 45° microphone position the model-scale BVI levels tend to be increased slightly, and the high-speed impulsive noise levels decrease slightly

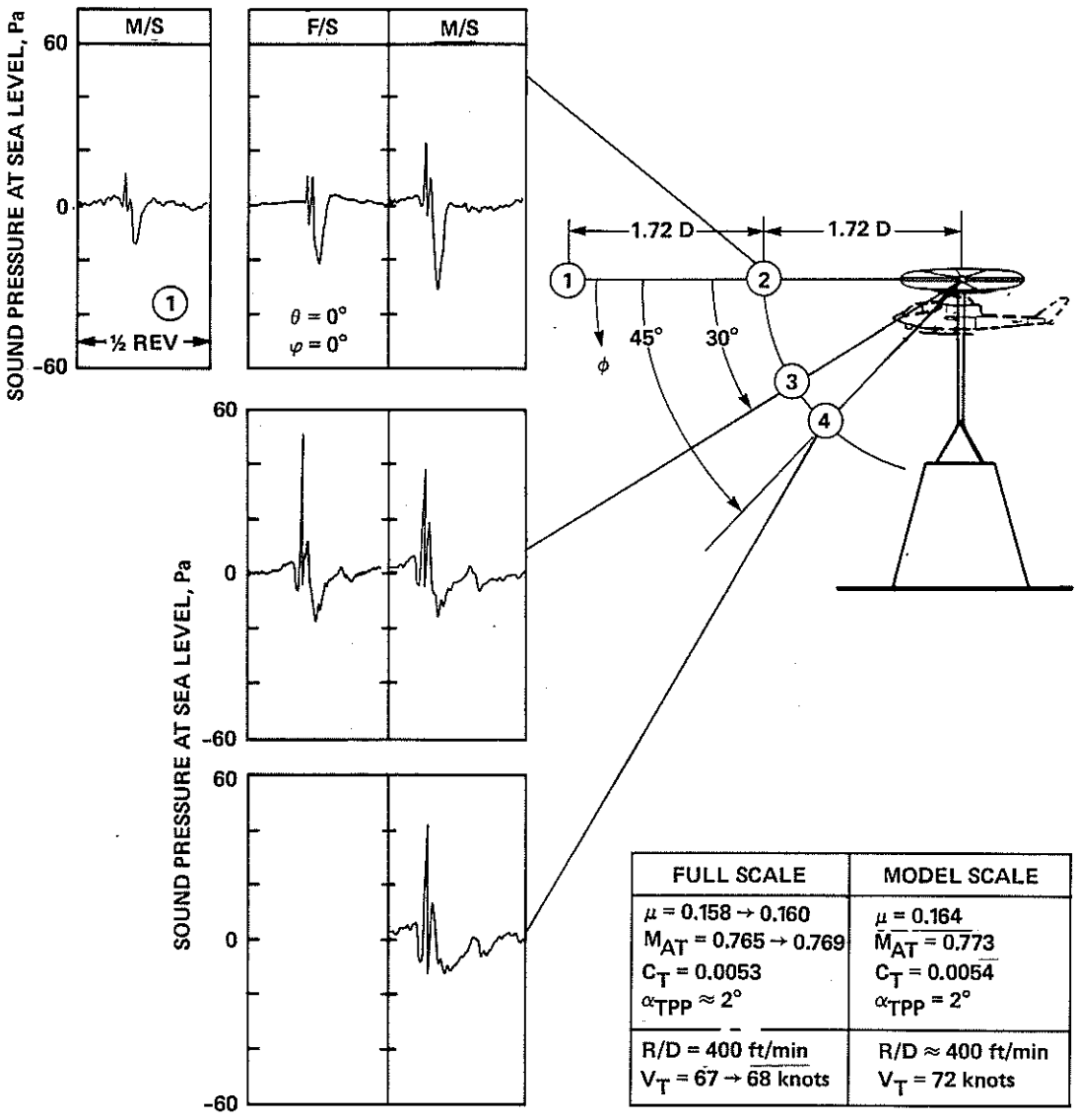

(a) Longitudinal directivity.

Figure 8. Comparison of model-scale and full-scale noise directivity.

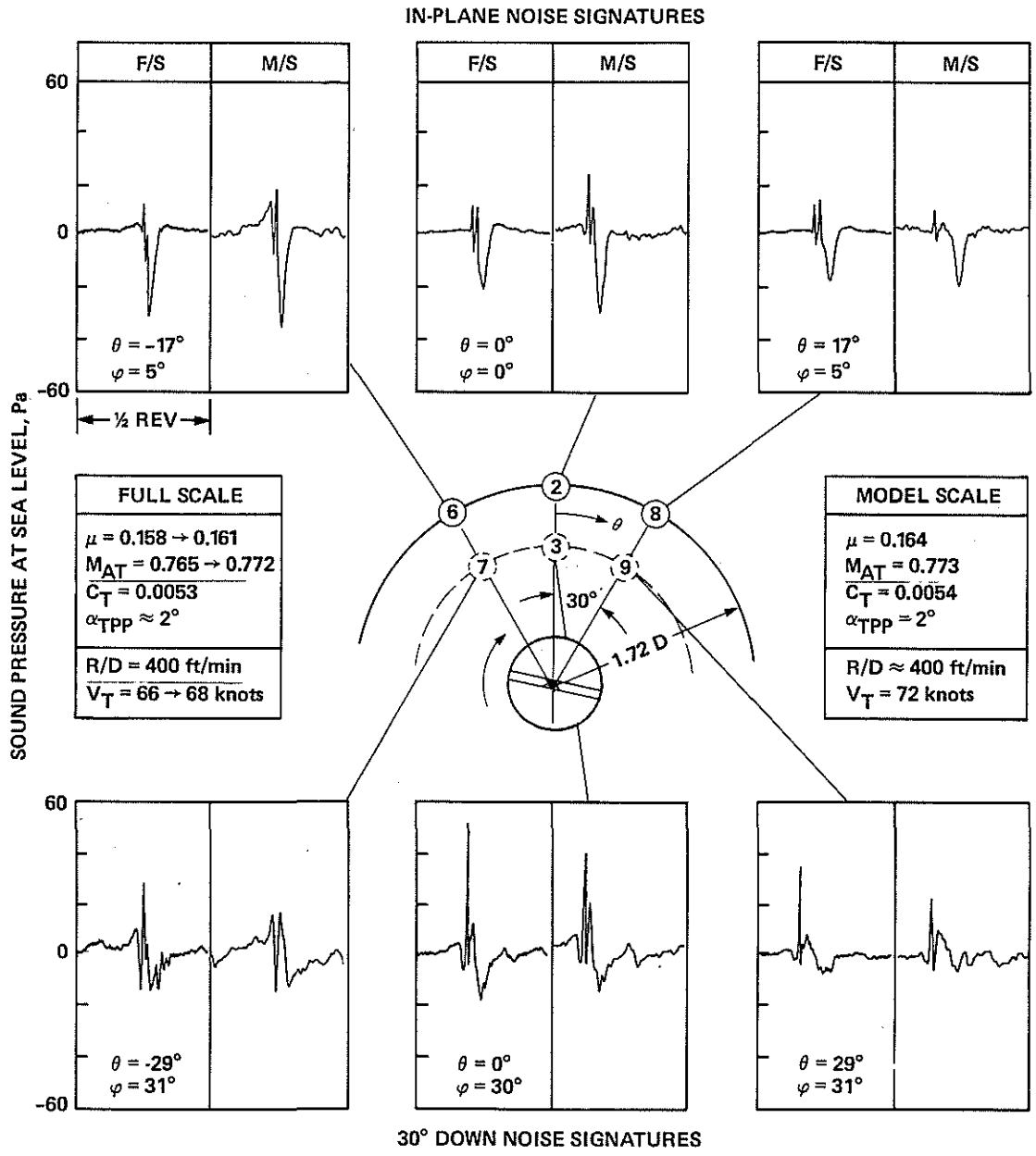

(b) Lateral directivity.

Figure 8. Concluded.

from the 30° microphone position. However, all trends observed over the parametric sweep are similar for either microphone location.

The results for the low advance ratio case ($\mu = 0.164$) are shown in figure 9. The averaged model-scale pulses are remarkably similar and consistent over the entire range of tip-path-plane angles considered. At negative tip-path-plane angles, corresponding to climbing flight, two small BVI impulses are seen. As the tip-path-plane angle is made more positive (simulating decreasing rates of climb), the first of these two impulses grows in magnitude, reaching a maximum at $\alpha_{TPP} = 0°$. At more positive tip-path-plane angles, the magnitude of this large pulse gradually decreases, and the BVI waveform gradually changes to three positive impulses. The third impulse precedes the other two and, although growing with increasing α_{TPP}, it is smaller in amplitude. The averaged full-scale data exhibit almost the same trends with rate of descent. However, the maximum averaged value of BVI occurs at a rate of descent of 400 ft/min, which corresponds to an estimated tip-path-plane angle of 2° (instead of 0° from the model-scale tests).

The maximum amplitude BVI model-scale and full-scale waveforms are plotted on a larger scale in the lower half of figure 9 for $\mu = 0.164$. The amazing similarity of pulse shape and amplitude are rapidly apparent. Even the smaller details of the two waveforms match remarkably well. However, on very close inspection, the pulse widths of the full-scale data are, in general, smaller than those of the model scale data. This suggests that the average vortex-core sizes of the trailing vortex system of the full-scale rotor are smaller than the corresponding model-scale vortex cores. Although the average values of model-scale and full-scale BVI match very well, it should be remembered that sudden bursts of large amplitude, full-scale BVI occur (see fig. 7). As shown in figure 9, sudden variations in tip-path-plane angle cannot, by themselves, explain this phenomenon in model scale. The maximum amplitudes of the model-scale BVI tests never exceeded the average value shown by more than 10%. However, as already noted (fig. 7), the maximum amplitudes of the full-scale data exceeded the average full-scale values by as much as 50%. This discrepancy is thought to be real and is hypothesized to be related to the different vortex structures of the model-scale and full-scale wake systems.

Similar results are found when the model scale and full scale are compared for $\mu = 0.194$ (fig. 10). Good general agreement in pulse shape exists for the peak values of BVI noise. However, the pulse widths of the full-scale BVI waveforms are again smaller than the model-scale.

The agreement between model-scale and full-scale averaged data begins to deteriorate for $\mu = 0.224$, as shown in figure 11. However, the envelope of the averaged acoustic data exhibits a fine structure that is just barely noticeable in model-scale.

This discrepancy is dramatically illustrated in figure 12 for the $\mu = 0.270$ case. Model-scale averaged waveforms exhibit smooth, consistent BVI patterns for the entire range of tip-path-plane angles. In simulated level, steady-state flight ($\alpha_{TPP} = -4°$), two BVI pulses are measured. As the tip-path-plane angle is increased, the amplitudes of these increase slightly, and they are joined by a third, small-amplitude

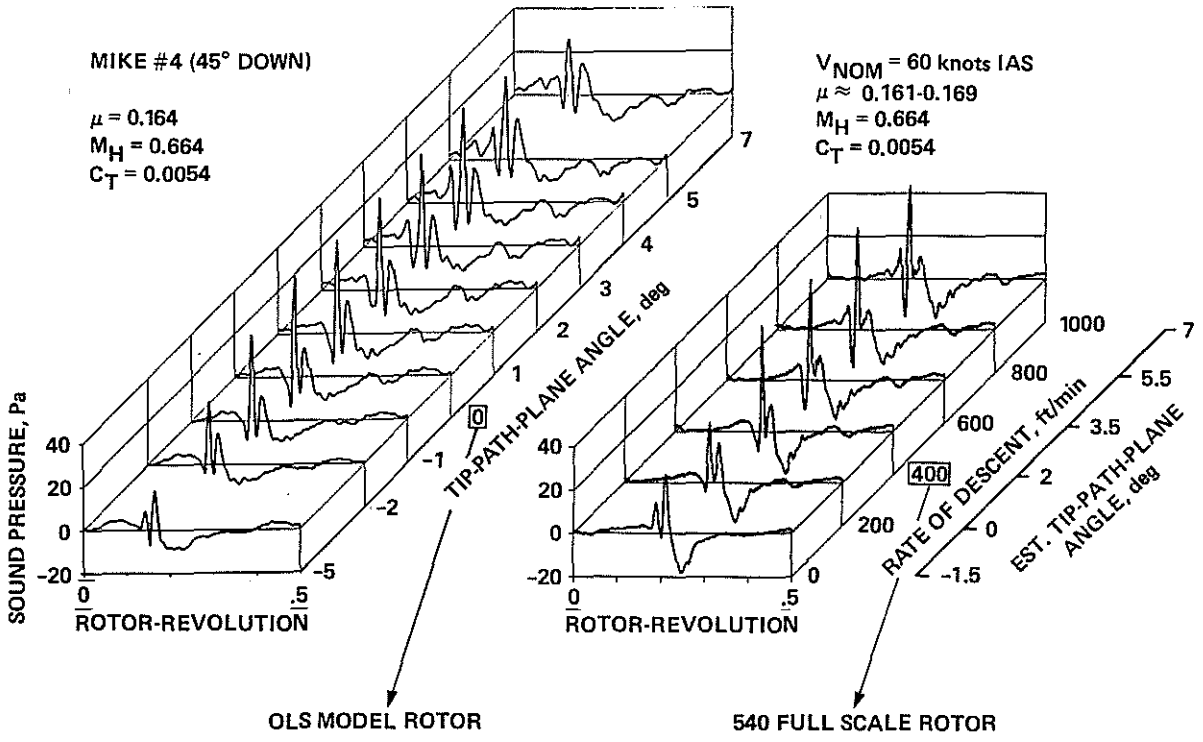

(a) Sweep of tip-path-plane angle or rate of descent.

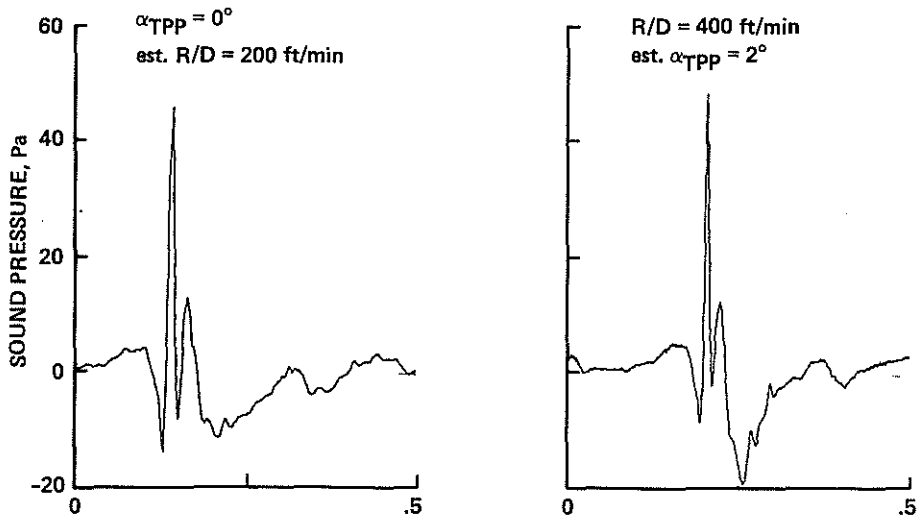

(b) Waveform comparisons of most intense interaction.

Figure 9. Comparisons of model-scale and full-scale acoustic data: μ = 0.164.

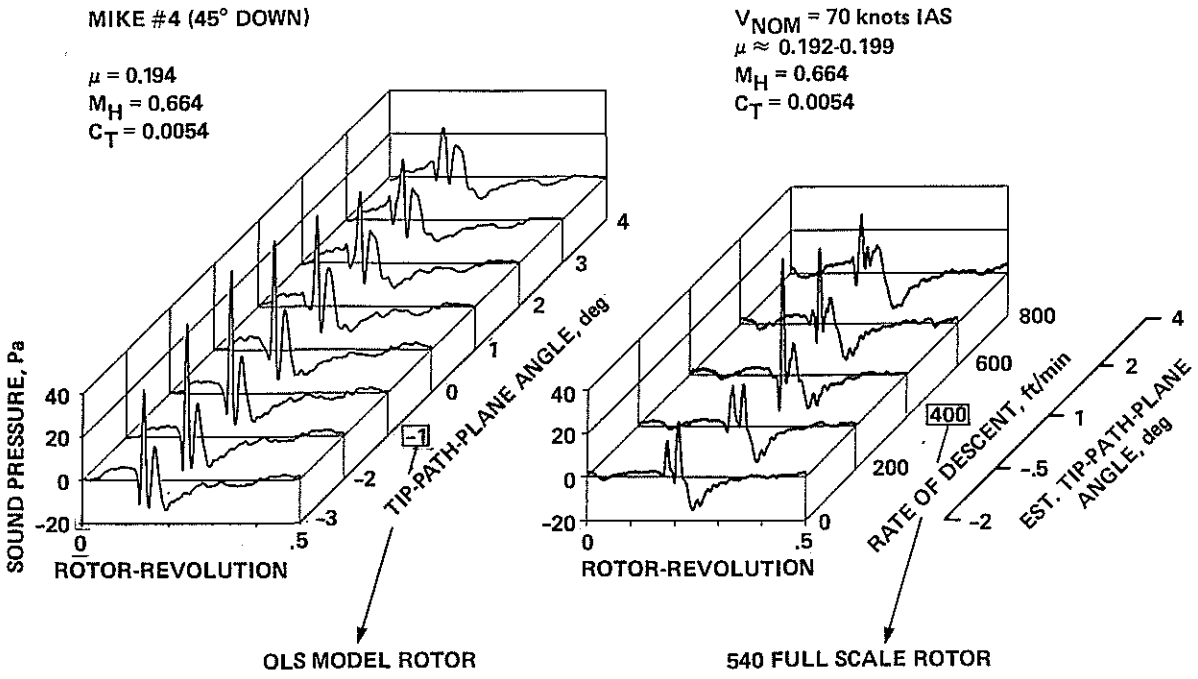

(a) Sweep of tip-path-plane angle or rate of descent.

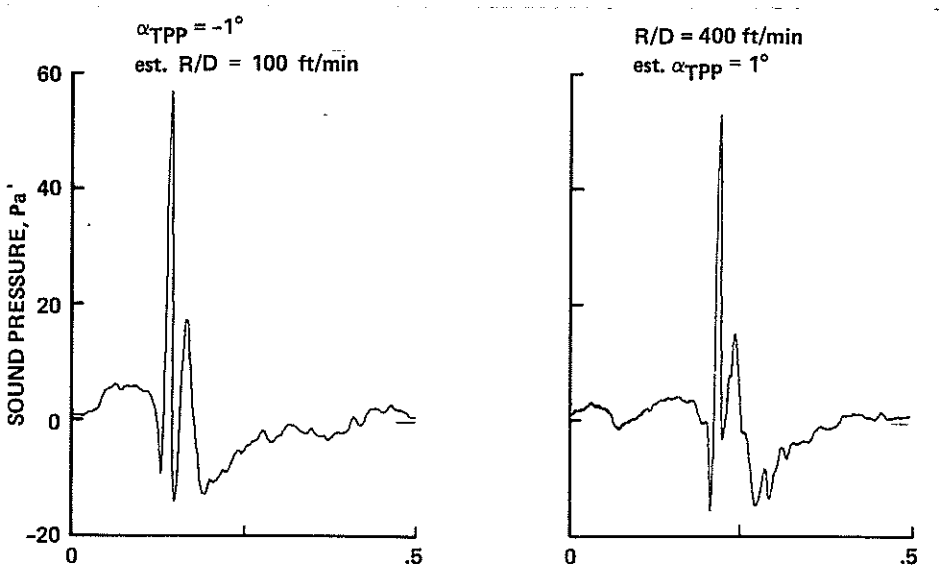

(b) Waveform comparisons of most intense interaction.

Figure 10. Comparisons of model-scale and full-scale acoustic data: μ = 0.194.

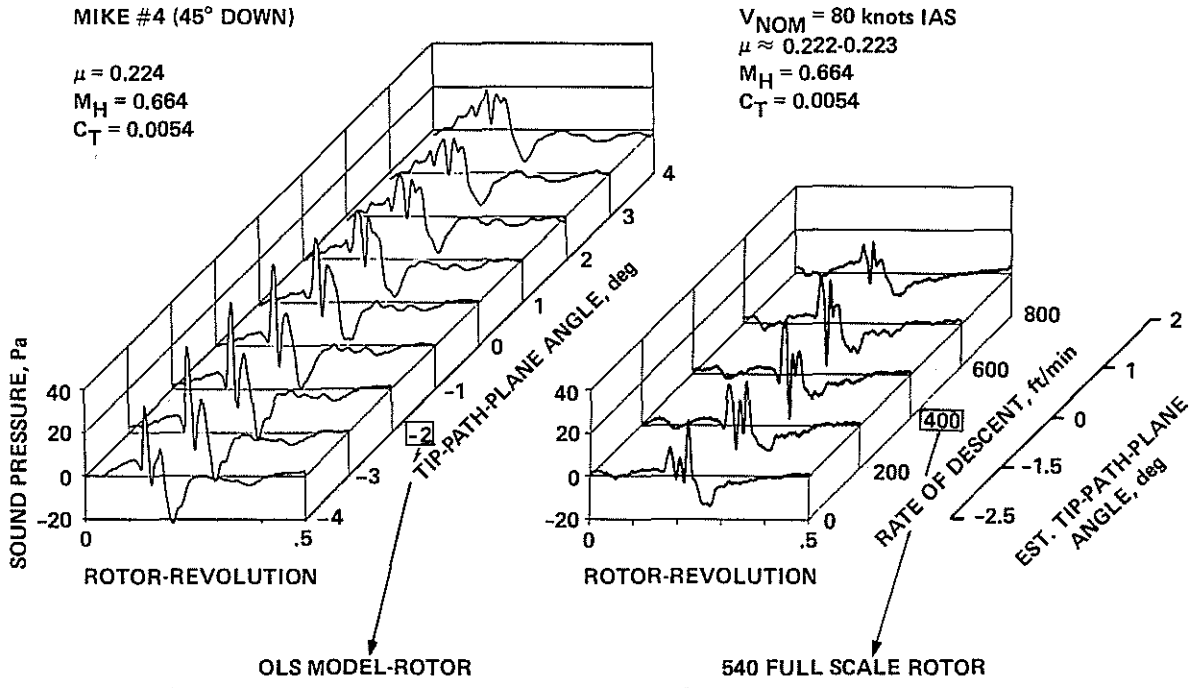

(a) Sweeps of tip-path-plane angle or rate of descent.

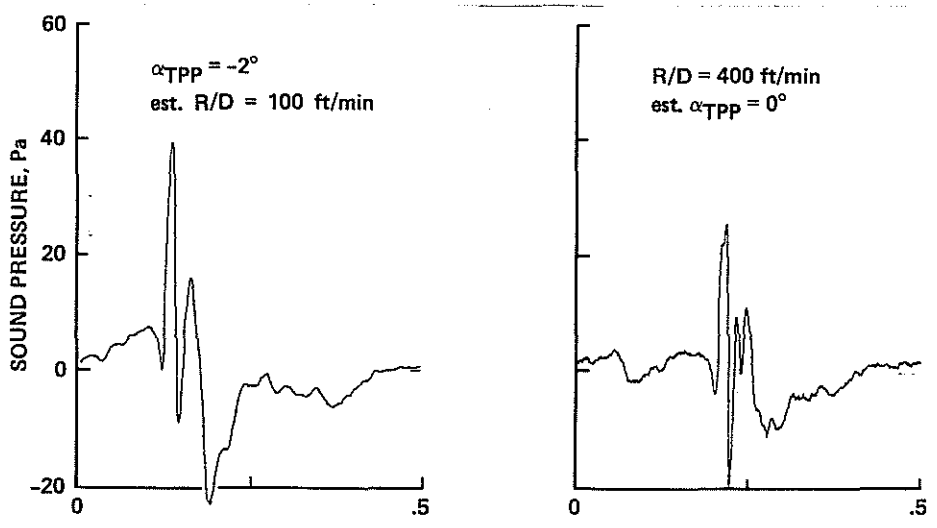

(b) Waveform comparisons of most intense interaction.

Figure 11. Comparisons of model-scale and full-scale acoustic data: μ = 0.224.

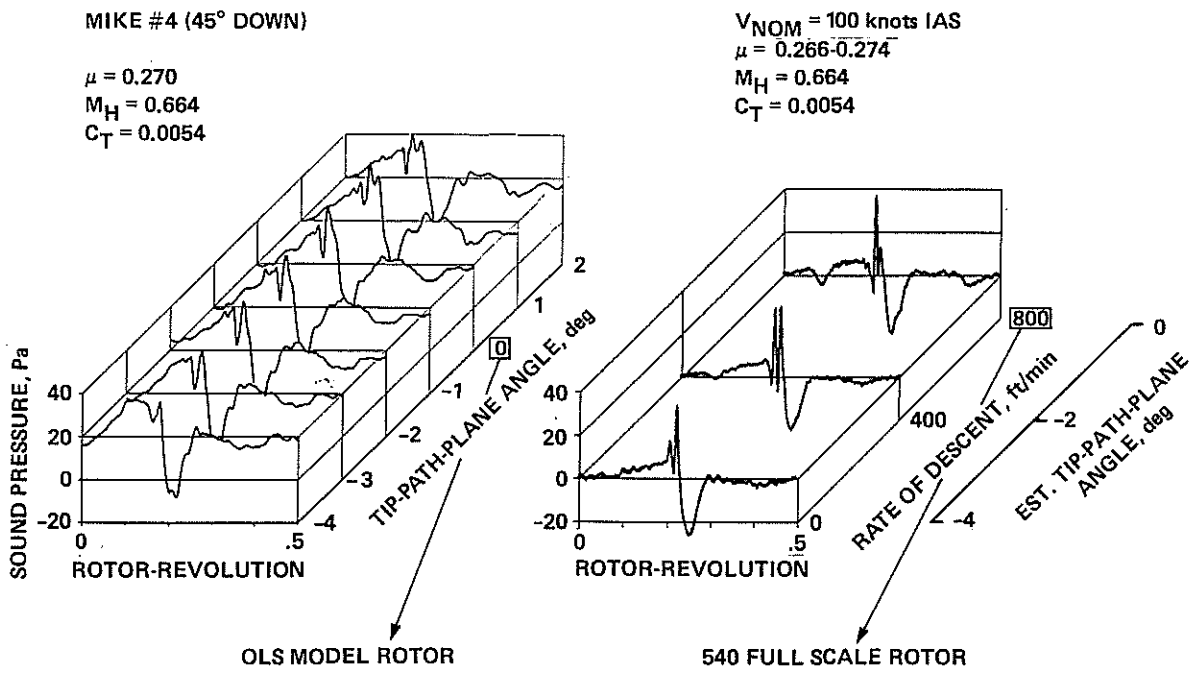

(a) Sweep of tip-path-plane angle or rate of descent.

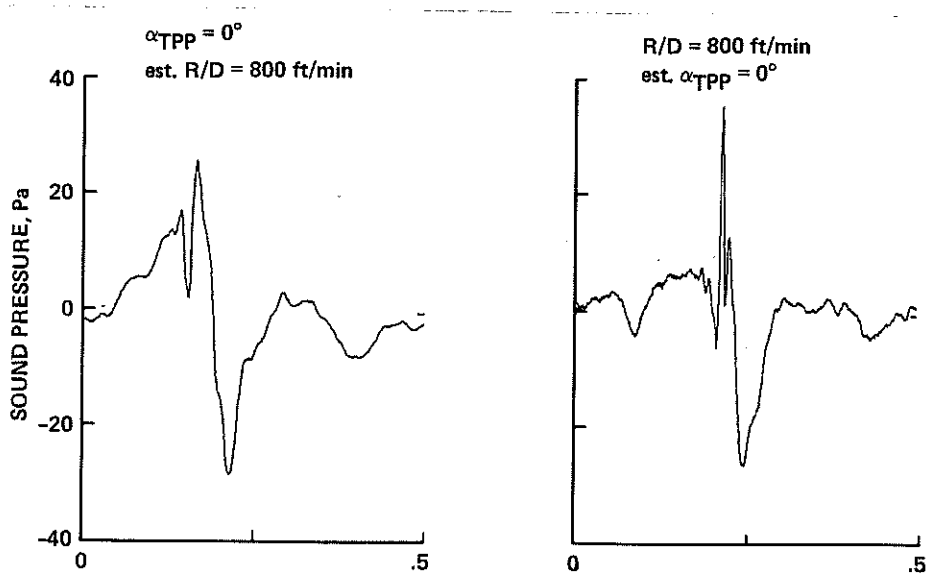

(b) Waveform comparisons of most intense interaction.

Figure 12. Comparison of model-scale and full-scale acoustic data: μ = 0.270.

pulse. The full-scale averaged waveforms look quite different. They are dominated by two rather intense BVI pulses whose pulse widths are about one half to one third that of the model-scale data. The amplitude of these full-scale pulses is, in general, larger than that shown in the smoother model-scale data. A comparison of these differences is seen quite clearly in the lower half of figure 12 where the maximum amplitude BVI model-scale and full-scale pulses are compared. The full-scale BVI data contain two sharp BVI pulses just before the large negative high-speed impulsive-noise pulse. The model-scale data have a single pulse, occurring at the same time, whose average amplitude is about one third smaller and slightly wider than the sum of the pulse widths of the full-scale data.

At first glance, the model-scale BVI data look as if they have been unintentionally filtered. However, as mentioned in an earlier part of this paper, the frequency response of the recording and analysis equipment was maintained at 20,000 Hz. This should be more than adequate for faithful reproduction of BVI model-scale events whose pulse widths are about 0.5 msec.

At the present time, we do not know for certain why the pulse-shape details of the model-scale and full-scale data do not agree at higher advance ratios. Differences in the wake-vortex structure resulting from vastly different Reynolds numbers or from full-scale piloting inputs or both are possible mechanisms. It is hoped that a careful reduction of the model-scale pressure data and an associated comparison of full-scale pressure data under similar conditions will help resolve the noted differences.

6. SOME PARAMETRIC VARIATIONS

Once it has been demonstrated that the acoustic phenomena of interest are scalable, wind-tunnel testing can be used to explore wide ranges of test conditions in a controlled environment. This is in contrast to in-flight full-scale testing, for which safety of flight considerations and piloting techniques limit the choice of conditions that can be flown. In this paper, we have shown that model-scale wind-tunnel testing does duplicate the full-scale measured acoustic events at the lower advance ratios ($\mu = 0.164$). Therefore, the effect on radiated noise of changes in thrust and hover tip Mach number is presented for this case.

The change in average BVI noise level with changing thrust levels is shown in figure 13 for a constant tip-path-plane angle ($\alpha_{TPP} = 1°$). The peak pressure spike of the largest BVI rises almost linearly with thrust, almost doubling for a doubling of thrust coefficient. The largest negative impulse rises much faster, suggesting that the interaction phenomenon is changing character at higher thrust levels.

Some care must be exercised when interpreting the data in figure 13. As thrust is increased, there is an increase in the average inflow to the rotor which increases the effective separation distance between the rotor tip-path plane and the shed tip-vortex system. To maintain the same separation distance, the rotor tip-path-plane angle

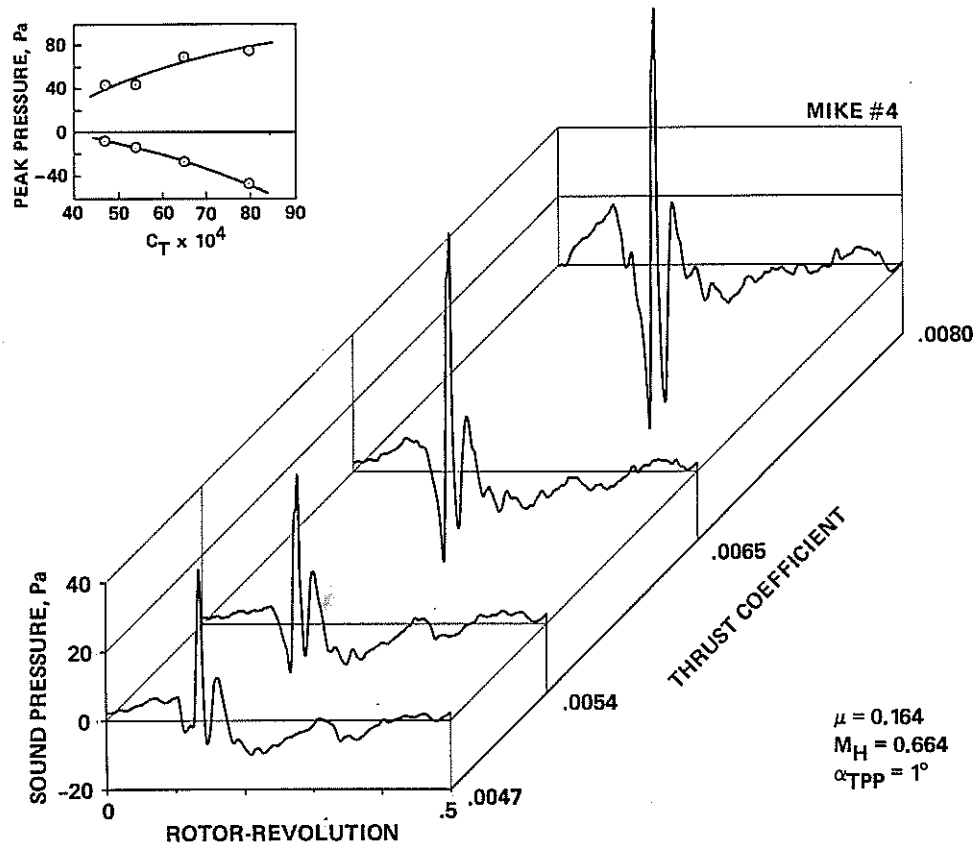

Figure 13. Effect of thrust variation.

should be increased (made more positive), thus effectively reducing this increased inflow resulting from increased thrust.

A method of estimating the change in BVI impulsive noise with changing thrust levels that attempts to account for this effect is shown in figure 14. First, the maximum positive peak pressure level is found for the largest BVI pulse for all possible tip-path-plane angles at a fixed advance ratio and a fixed tip Mach number at hover. This peak pressure value is then plotted as a function of thrust. As explained above, the tip-path-plane angle at which maximum levels of BVI occur, increases with increasing C_T, as indicated in figure 14. The peak amplitude of BVI impulsive noise is increased slightly over that shown in figure 13 for a constant tip-path-plane angle of +1°.

The change in BVI impulsive noise with changes in hover Tip Mach number, M_H, is shown in figure 15 for $\mu = 0.164$, $C_T = 0.0054$, and $\alpha_{TPP} = +1°$. Because μ is constant, a variation in M_H is equivalent to a variation in the advancing-tip Mach number M_{AT}, which has been added as a second scale. Large increases in the peak values of the

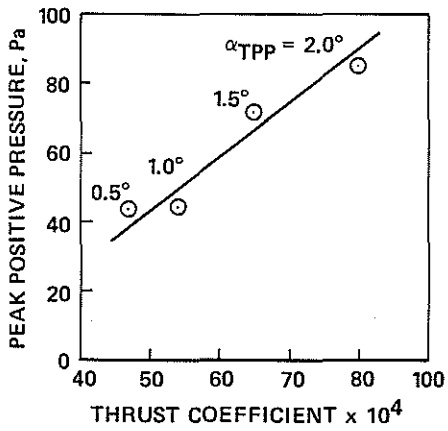

Figure 14. Peak positive pressure versus thrust coefficient.

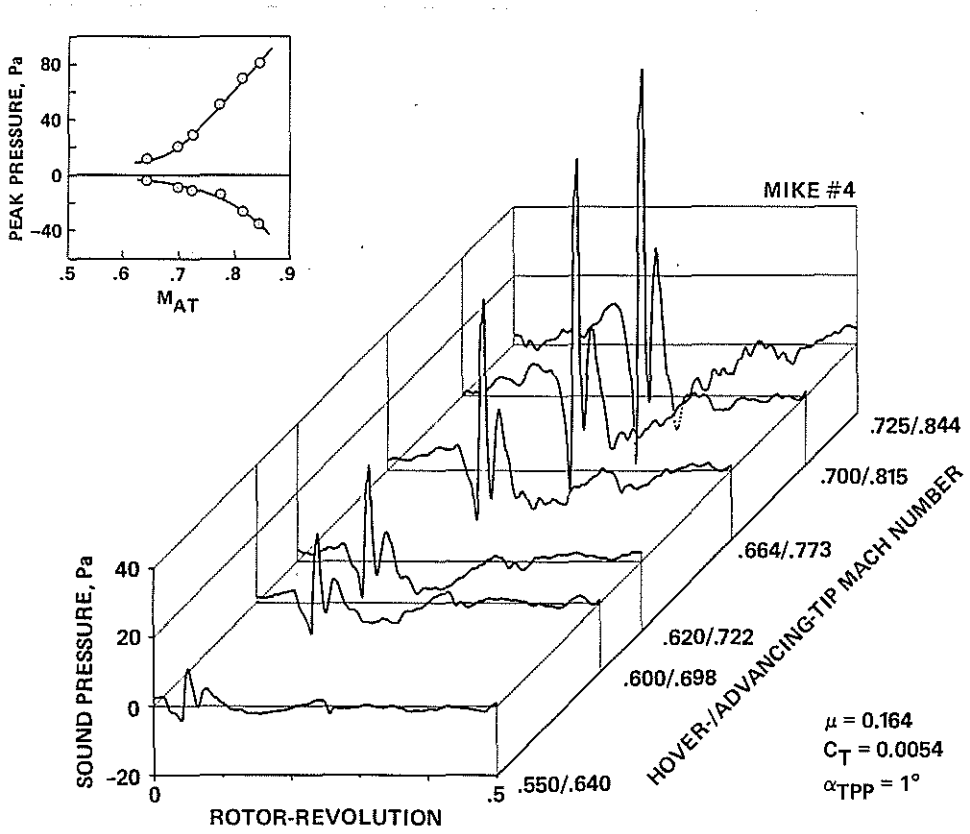

Figure 15. Effect of blade-tip Mach number.

positive and negative pulses occur, demonstrating that hover tip Mach number is one of the most sensitive design parameters of BVI impulsive noise.

There are at least two known factors which combine to make BVI impulsive noise sensitive to M_H. For example, it can be argued that increasing M_H at constant thrust coefficient increases the real thrust

on each blade, thus increasing the strength of the tip vortices that are shed. However, because the rotor is operating at higher tip velocities, the change in angle of attack (and in perturbation pressure coefficient, ΔCp), induced by the stronger tip-vortex system, remains fairly constant. Therefore, the BVI impulsive noise levels increase as the hover tip Mach number increases, because the absolute values of perturbation pressure increase in direct proportion to the velocity of the rotating blades. It was also shown in reference 13 that the acoustic levels of BVI in certain radiation directions are strongly related to the "trace Mach number" of the interaction. Because the trace Mach number changes with changes in the hover tip Mach number, BVI impulsive noise levels can be increased or decreased, depending on the geometry of the interaction process and the far-field location of the measurement microphone. The values of peak BVI impulsive noise levels shown in figure 15 are undoubtedly influenced by both of these factors.

7. CONCLUDING REMARKS

Acoustic data taken in the world's largest anechoic wind tunnel—the DNW in the Netherlands—have documented the blade-vortex interaction (BVI) impulsive noise radiated from a 1/7-scale main-rotor model of the AH-1 series helicopter. The model-scale data were compared with full-scale in-flight acoustic data under similar operating conditions. The major findings of the work to date are as follows:

1. A new method of averaging the acoustic data gathered by in-flight station-keeping methods has been developed that successfully extracts the average BVI noise from that of sources other than the main rotor emitted by the helicopter. The method was successfully used to document average levels and time-histories of BVI noise emitted by the AH-1S helicopter over a full range of flight conditions. The bothersome tail-rotor periodic noise was eliminated from the BVI data, thus allowing a careful interpretation of detailed waveform characteristics of the main-rotor impulsive noise.

2. A set of nondimensional scaling equations was used to establish and test a matrix of model-scale BVI conditions that were compatible with full-scale BVI conditions. Advance ratio, hover tip Mach number, thrust coefficient, and local inflow ratio are the important nondimensional parameters. Major directivity profiles of the radiated noise were documented at an advance ratio of 0.164, confirming that BVI noise is a collection of highly directional phenomena. The peak values of BVI noise are radiated predominately 30° to 45° below the rotor plane in the direction of forward flight.

3. At low advance ratios (μ = 0.164-0.194), the average BVI acoustic data for the 1/7-scale model duplicated the average full-scale BVI noise data remarkably well. Average peak amplitudes and waveform shapes were duplicated for a wide range of microphone locations. Pulse widths of the full-scale BVI impulses were slightly smaller than model-scale pulse widths, suggesting that the tip vortices shed from the full-scale rotor had smaller viscous cores.

4. At moderate advance ratios (μ = 0.224-0.270), the model-scale BVI acoustic results did not duplicate the full-scale data very well. Although the general low-frequency shape of the waveform was similar, amplitude and waveform details of the BVI pulses were notably different. The full-scale BVI data had large, sharp BVI pulses that were not seen in model-scale under similar nondimensional conditions.

5. Full-scale BVI acoustic data exhibited an unsteadiness in level not seen in the model-scale data taken in the DNW. All of the model-scale data were very steady under all of the operating conditions reported.

The good agreement at low advance ratios and the lack of agreement between model-scale and full-scale BVI data at moderate advance ratios is the most puzzling finding of this study. At the present time, no substantiated explanation of this disagreement can be offered. Future efforts will use acoustic triangulation and cross-correlation of blade pressures with far-field acoustics to help explain why the model-scale and full-scale BVI acoustic waveforms disagree at these moderate advance ratios.

ACKNOWLEDGMENTS

The authors thank their many friends at the U.S. Army Aeromechanics Laboratory, DFVLR, and the DNW for their extraordinary efforts on this project. In particular, we would like to thank Ozzie Swenson for his assistance with the electronics in developing the in-flight averaging procedure. We also would like to acknowledge the help of John Davis in providing the C-81 trim calculations shown in the paper.

REFERENCES

1) F. H. Schmitz, and Y. H. Yu: Helicopter Impulsive Noise: Theoretical and Experimental Status. NASA TM-84390, 1983.

2) W. R. Splettstoesser, K. J. Schultz, F. H. Schmitz, and D. A. Boxwell: Model Rotor High-Speed Impulsive Noise— Parametric Variations and Full-Scale Comparisons. Presented at the 39th Annual National Forum of the American Helicopter Society, St. Louis, Mo., May 1983.

3) D. A. Boxwell, F. H. Schmitz, W. R. Splettstoesser, and K. J. Schultz: Model Helicopter Rotor High-Speed Impulsive Noise: Measured Acoustics and Blade Pressures. Paper No. 17, 9th European Rotorcraft Forum, Stresa, Italy, Sept. 1983.

4) C. Cox: Development of Piloting Techniques to Reduce Helicopter Approach Noise. Paper No. A-84-40-04-D000, 40th Annual National Forum of the American Helicopter Society, Arlington, Va., May 1984.

5) D. A. Boxwell, and F. H. Schmitz: Full-Scale Measurements of Blade-Vortex Interaction Noise. J. Am. Helicopter Soc., Vol. 27, No. 4, Oct. 1982.

6) C. R. Cox: Rotor Aerodynamic and Aeroacoustic Environments. AIAA Paper 77-1338, 1977.

7) F. H. Schmitz, D. A. Boxwell, S. Lewy, and C. Dahan: Model-to-Full-Scale Comparisons of Helicopter Blade-Vortex Interaction Noise. J. Am. Helicopter Soc., Vol. 29, No. 2, Apr. 1984.

8) F. H. Schmitz, and D. A. Boxwell: In-Flight Far Field Measurement of Helicopter Impulsive Noise. J. Am. Helicopter Soc., Vol. 21, No. 4, Oct. 1976.

9) D. A. Boxwell, and F. H. Schmitz: In-Flight Acoustic Comparison of the 540 and K747 Main Rotors for the AH-1S Helicopter. Appendix to U.S. Army Aviation Engineering Flight Activity Report 77-38, Edwards AFB, Calif., Oct. 1979.

10) R. E. George, and V. Duffy: In-Flight Measurement of Aircraft Acoustic Signals. Proceedings of the 23rd International Instrumentation Symposium, Vol. 14, Advances in Test Measurement, Las Vegas, Nev., Nov. 1977.

11) J. C. A. Van Ditshuizen, G. D. Courage, and R. Ross: Acoustic Capabilities of the German-Dutch Wind Tunnel, DNW. Paper No. 9.5, 8th European Rotorcraft Forum, Aix-en-Provence, France, 1982.

12) James R. VanGaasbeek: Rotorcraft Flight Simulation Computer Program C81 with DATAMAP INTERFACE, USAAVRADCOM-TR-80-D-38A, Oct. 1981.

13) Y. Nakamura: Prediction of Blade-Vortex Interaction Noise from Measured Blade Pressure. Paper No. 32, Seventh European Rotorcraft and Powered Lift Aircraft Forum, Garmisch-Partenkirchen, Federal Republic of Germany, 1981.